Diffusion driven layer-by-layer assembly of graphene oxide nanosheets into porous three-dimensional macrostructures

Jianli Zou, Franklin Kim*

Institute for Integrated Cell-Material Sciences (WPI-iCeMS), Kyoto University, Kyoto 606-8501, Japan

* E-mail: fkim@icems.kyoto-u.ac.jp

ABSTRACT

Despite the strong progresses in preparing numerous types of nanosheets, it remains a difficult challenge to assemble the tiny building blocks into functional macroscale architectures suitable for practical applications. Herein, we introduce a diffusion driven layer-by-layer assembly and demonstrate its application for the construction of graphene oxide sheets into various three-dimensional structures. This process involves complexation of the negatively charged graphene oxide sheets and positively charged branched polyethylenimine at a given interface. Interestingly, we find that the diffusion of branched polyethylenimine molecules allows the complex to continuously grow into foam-like frameworks with tunable porosities. Furthermore, the assembly process is quite robust and can be utilized in various configurations such as to create free-standing architectures with tailored shapes or patterned films on a substrate. With such useful features, we believe that this technique will be able to serve as a valuable tool for the assembly of nanomaterials.

Significant development in both physical and chemical exfoliation techniques during the past several years has allowed the production of nanosheets from a wide range of layered materials, including graphite, transitional metal dichalcogenides, oxides, and tertiary carbides and nitrides.[1-7] The nanosheets are sought after for various applications such as ultra-capacitors, battery electrodes, filtration membranes, and sensors.[8-15] However, in order to integrate the nanosheets into such real-life devices it is often necessary to construct them into suitable two-dimensional (2D) or three-dimensional (3D) macrostructures. As a result, developing methods to assemble the nanosheets with good control and efficiency becomes a critical challenge.

Forming nanosheets into thin-film structures can be generally done with good precision and simplicity using well-established strategies such as spin-coating,[16] filtration,[17,18] layer-by-layer (LbL) assembly,[19,20] and Langmuir-Blodgettry.[21,22] On the other hand, creating thicker structures has been a more difficult task. An important characteristic of nanosheets is its high-surface area. However, the nanosheets can easily aggregate during assembly, leading to significantly decreased surface area and thus diminished material properties. Therefore, the main question becomes how to construct the nanosheets into 3D macrostructures while suppressing aggregation. Few promising directions have been explored to address this issue, especially using graphene oxide (GO) nanosheets. For example, several researchers have demonstrated hydrothermal treatment of GO suspension as a versatile method to produce various types of porous graphene frameworks.[23-26] Vermant et al. reported the preparation of GO frameworks from bi-continuous emulsions which surface are stabilized by the nanosheets.[27] Niu et al. introduced a leavening process, showing that tightly packed GO films

3

can be inflated into a foam-like structure by the gas evolution during reduction of GO.[28] Inclusion of spacers between the GO layers, such as nanoparticles or polymer beads, has also been widely investigated.[11,29,30] Such developments have opened new ways to obtain diverse graphene-based macrostructures that exhibit favorable properties for applications such as sensors and energy storage. On the other hand, it remains a difficult challenge to direct the construction of nanosheets with good control over the shape of the assembled structure. For instance, molding the GO into tailored forms, such as sphere, cube, and fiber, is not as straightforward to achieve using conventional methods and generally requires elaborate experimental setups. Another example would be growing thick graphene films at selected pre-patterned area of a given substrate, which is potentially important for device fabrication purposes. Furthermore, the aforementioned assembly techniques mostly rely on the inherent characteristics of GO, and therefore is unlikely to be easily applicable to the assembly of different types of nanomaterials.

We previously reported a strategy for directing the assembly of nanosheets into various macrostructures through interfacial polyionic complexation.[31] A key point of the study was that nanosheets often behave as charged macromolecules and therefore can form a stable complex with oppositely charged polyelectrolytes. Such characteristic was explored using chitosan, a positively charged biopolymer, which readily interacted with nanosheets that have negative surface charges such as GO, WS_2, and MoS_2. We found that the complexation could be confined at liquid-liquid or air-liquid interfaces, which allowed control over the nanosheet assembly into forms such as films, fibers, and capsules. These results suggest that interfacial polyionic complexation could be a useful tool for guiding the assembly of nanosheets in a

4

simple way. At the same time, we noticed that the nanosheet/chitosan complex typically stops growing after reaching a thickness of few tens of nanometers, which is due to the layer acting as a barrier that blocks further reaction. This has been a limiting factor in tuning the assembly process, especially for creating thicker macrostructures.

Herein, we report a completely different assembly behavior that was observed during the complexation between GO and branched poly (ethyleneimine) (b-PEI). In contrast to the case of chitosan, b-PEI is able to diffuse through the GO/b-PEI complex formed at the interface, which allows the layer to grow in a continuous fashion into 3D structures with thickness reaching millimeter ranges. Furthermore, the assembled structures display a foam-like porous feature. The GO/b-PEI structure formation occurs in a way that resembles a layer-by-layer assembly. On the other hand, rather than requiring multiple deposition steps, the assembly is driven by diffusion of b-PEI and therefore, once initiated, can progress without additional external force or stimuli. Based on such observations, we propose a new type of assembly method, namely "diffusion driven layer-by-layer assembly", or "dd-LbL". This process is quite robust and can be utilized in various ways to create a wide range of macrostructures. For example, in this report we demonstrate the assembly of GO nanosheets into porous frameworks with adjustable porosity, growth of patterned multilayered films on solid and flexible substrates, and preparation of free-standing 3D structures which shape can be controlled through the use of templates. With such set of useful capabilities, we strongly believe that this "diffusion driven LbL assembly" will be able to serve as a versatile technique for constructing nanosheets into diverse 3D macrostructures.

Results

Diffusion driven layer-by-layer assembly of GO and b-PEI. Polyethylenimine (PEI) is a positively charged polyelectrolyte which contains amine functional groups. It is used in various industrial applications such as paper production, detergent, and water treatments. PEI is commercially available in both linear and branched forms. However, due to limited solubility of linear PEI in water at room temperature, we focus mainly on branched PEI for this study.

To examine the interaction of b-PEI and GO at a liquid-liquid interface, droplets of a b-PEI solution (M_w = 750,000, M_n = 60,000, 25 wt. % in water, ~ 12 μl) were added to a GO suspension (8 mg ml^{-1} in DMF:water = 9:1 mixture) and left for several hours (Figure 1a). This induced complexation of GO and b-PEI at the droplet surface, which was demonstrated by the formation of a dark brown layer surrounding the droplet (Figure 1b). Interestingly, the size of the sphere became significantly larger compared to the initial b-PEI droplet, showing a diameter increase from 2.8 mm to around 6.5 mm. Furthermore, the layer was sufficiently stable enough such that the wet structure could preserve its spherical shape even after being left in air or manipulated by a pair of tweezers. For simplicity, we will call this product GO/b-PEI bead. Cutting the bead with a razor blade revealed that the shell thickness was in the range of several millimeters (Figure 1c). Further in-depth structure of the GO/b-PEI complex layer was investigated by SEM (Figure 1d – f). For sample preparation, the bead was dried by freeze-drying to minimize structural changes. SEM images show that the GO nanosheets formed a highly porous network, suggesting that the initial wet structure contained a large

6

volume of water. In addition, the nanosheets are mostly arranged in a layered configuration despite the large voids, forming an onion-like architecture composed of numerous concentric shells. It should be noted that drying the sample in an oven or in air lead to substantial structural changes, likely due to surface tension of the water pulling the GO sheets together during evaporation. In fact, such phenomena could be utilized as a way to adjust the porosity of the assembled structure, as will be discussed in more detail below.

XRD analysis of the GO/b-PEI bead shows a peak at a smaller angle ($2\theta = 5.39°$, $d = 1.64$ nm) compared to a solid sample of unmodified GO ($2\theta = 10.57°$, $d = 0.84$ nm) (Figure 1g, Supplementary Fig. 1). Such increase in interlayer spacing suggests that b-PEI becomes incorporated between the GO layers during the assembly process. FT-IR spectrum of GO shows peaks at 1730 cm^{-1} from C=O (carbonyl) stretching and 1626 cm^{-1} from C=C (aromatic) stretching (Supplementary Fig. 2). However, the carbonyl peak becomes no longer noticeable after complexation with b-PEI. In addition, characteristic peak from the amine group of b-PEI (1659 cm^{-1}) is also not observed from the complex (Supplementary Fig. 2). This suggests that the carbonyl group of GO and amine group of b-PEI is strongly interacting with each other, leading to peak shifts overlapping with the broad C=C peak.

Based on such observations, we propose the following mechanism for the bead formation (Figure 1h). As the b-PEI droplet is immersed into a GO suspension, complexation between the polyelectrolyte and nanosheets occurs at the interface due to electrostatic interactions. This produces a thin complex layer encapsulating the droplet, which outer surface is dominated by negatively charged GO. Despite such layer formation, b-PEI is able to

7

penetrate the barrier and continuously diffuse out through the interspace between GO sheets, most likely driven by osmotic pressure. Some of the diffused b-PEI attaches to the negatively charged outer surface, leading to additional deposition of GO onto the shell. At the same time, this leads to depletion of GO in the vicinity, which allows the other portion of b-PEI to diffuse further out and create a new interface apart from the initial complexation layer, resulting in the large void between layers. This cycle of complexation – diffusion – complexation allows continuous formation of GO shells around the b-PEI droplet, eventually building up the layered and porous 3D macrostructures shown in Figure 1. It should be noted that the reactants are continuously consumed as the assembly progresses. This is likely to lead to decreased frequency of complexation and thus slower growth of the assembled structure with time. Indeed, we observe that although the size of the GO/b-PEI beads does increase with longer reaction time, not much change is noticed after 24 hours (Figure 1i).

Our proposed assembly model is further supported by quantitative analysis on the GO/b-PEI layer growth (Supplementary Fig. 3). It can be noticed that while the thickness of the shell increases with time, size of the inner hollow core remains mostly unchanged from the initial b-PEI solution droplet. This matches well with our hypothesis that the GO/b-PEI complexation first occurs at the surface of the droplet (i.e. interface between the two solutions) and then grows towards the direction of the GO suspension due to b-PEI molecules traveling across the interface. Interfacial complexation induced within a transparent tube also confirms that the reaction mostly occurs on the GO side (Supplementary Fig. 4). Drop in growth rate of the GO/b-PEI layer with time is also clearly observed; this indicates that although the assembly is driven by the diffusion of b-PEI, other factors such as depletion of the reactants

8

can influence the growth of the assembled structure. Similar diffusion-induced development of complex layer has also been observed during interactions between oppositely charged small molecules at liquid-liquid interfaces; however, the formation of a porous multilayered structure shown in Figure 1 is quite unique, which we attribute to the relatively large size and highly anisotropic shape of the GO sheets.[32-34]

In a previous study we have explored the interaction between GO and chitosan under similar experimental setups.[31] The formation of GO/chitosan complex layer was still observed at the droplet surface; however, the layer thickness was very thin and did not grow beyond 100 nm. Results in Figure 1 suggest that a critical factor for the continuous assembly of nanosheets to occur is whether the polyelectrolyte can penetrate the initial complexation layer. Although we do not yet fully understand what requisites need to be satisfied for this, comparison between chitosan and b-PEI provides some insights. We believe that two factors may be of importance, which are 1) strength of the GO/polyelectrolyte and polyelectrolyte/polyelectrolyte interaction, and 2) solubility of the polyelectrolyte. Chitosan is a linear polysaccharide which contains large number of hydroxyl and amine groups. Therefore it can form strong hydrogen bonding not only with GO but also with other chitosan molecules. This is likely to result in formation of a tightly bound complexation layer. On the other hand, the interaction between branched polymer chains such as b-PEI is generally weaker than that of linear polymers due to steric hindrance. In addition, b-PEI only contains amine groups and therefore do not form hydrogen bonding with other b-PEI molecules. Therefore, we can presume that the complexation layer of b-PEI and GO to be more loosely bound, which allows b-PEI to diffuse through the barrier. Similar considerations play a role in regard to the electrolyte solubility.

9

Chitosan solution becomes viscous and gel-like even at comparatively low concentrations due to strong interactions and entanglement between the polymer chains. As a result, the highest concentration that we could test was 2 wt. %. On the other hand, b-PEI solutions can easily be prepared in high concentrations due to relatively weak intermolecular interactions. For example, results in Figure 1 were produced using a 25 wt. % solution. Higher polymer concentration can be translated into stronger osmotic pressure and thus faster diffusion. Indeed, when a 10 wt. % b-PEI solution was used the size of GO/b-PEI bead was noticeably smaller, and below that concentration the complexation layer did not form properly (Supplementary Fig. 5). This suggests that higher concentrations of polyelectrolyte solution may be another important requisite for the multilayered assembly to occur. However, there are several other factors that could influence the behavior of polyelectrolytes such as molecular weight, solvent, and pH, and further studies are needed to more accurately elucidate the assembly mechanism.

The process of building up multilayered structures through alternating layers of oppositely charged materials as depicted in Figure 1h shares some similarities with conventional LbL assembly. At the same time, rather than going through multiple deposition cycles, the assembly is driven by diffusion and as a result, once initiated, can progress in a continuous fashion without additional treatments. Therefore, we use a new term "diffusion driven layer-by-layer assembly" or "dd-LbL assembly" to describe this unique process. Despite its simplicity, this assembly technique is quite versatile and can be utilized in various ways to construct a wide range of graphene-based superstructures with adjustable properties and shapes, as will be discussed throughout the rest of this report.

10

Properties of the assembled GO/b-PEI structures. An interesting characteristic of the structures produced by dd-LbL assembly is that they exhibit foam-like porous features as displayed in the SEM images shown in Figure 1. The porosity and stability of the assembled products can be further demonstrated by a simple oil absorbing experiment. When a freeze-dried bead was placed on top of a pool of pump oil, it rapidly absorbed the oil up to 35 times its own mass (Figure 2a). The beads could be recycled by immersing them into hexane to drain the absorbed oil. After dried, the sample returned back to its initial weight while the spherical structure was well-preserved (Figure 2a, bottom right). There was no significant change in the oil absorbing capacity even after several cycles, which illustrates the stability of the porous structure (Figure 2b). In addition, the beads showed similar absorbing efficiency with other types of solvents such as toluene, olive oil, and chloroform (30, 28, and 34 times its own mass, respectively, Figure 2c).

Due to its porous nature, the assembled GO/b-PEI structures are quite light. For instance, the product shown in Figure 1 has a density of ~ 27 mg cm^{-3}, similar with that of "GO foams" produced through a leaving process as reported by Niu et al.[28] At the same time, the sample porosity can be further tuned with simple modifications to the experimental conditions. One such method is to adjust the GO concentration. In general, lower concentrations leads to structures with lower densities, or in other words, higher porosity, as shown in Figure 2d. The structural differences can be also confirmed by SEM, with samples prepared at GO concentrations of 3 mg ml^{-1} (Figure 2e) and 5 mg ml^{-1} (Figure 2f) clearly exhibiting looser networks compared to that prepared at 8 mg ml^{-1} (Figure 1). Such changes in porosity can be well explained by our proposed assembly mechanism. Even after b-PEI diffuses into the GO

11

suspension, the two components need to get into contact for the complexation to occur. At lower GO concentrations, b-PEI is likely to diffuse longer distances before eventually interacting with the nanosheets to form a stable complex, leading to a more loosely packed structure and larger macroscopic pores. This is in good agreement with the observed results. For the same reasons, we can also expect the overall size of the assembled structure to be larger at lower GO concentrations, which is indeed the case (Supplementary Fig. 6). The lowest concentration we were able to obtain a stable structure from was 3 mg ml^{-1}, which produced a sample with density of 5.6 mg cm^{-3}. This value is comparable to those of ultralight graphene frameworks produced by hydrothermal treatment of GO[25] or chemical vapor deposition on metal foams.[35]

It should be noted that the low density, highly porous structures discussed above were obtained when the samples were dried by freeze-drying. During this process, not much change was noticed in the overall size and shape of the product. On the other hand, even with samples prepared under identical experimental conditions, using different drying procedures can lead to substantial structural changes. For example, the GO/b-PEI layer which thickness was ~ 2 mm in its initial wet state (Figure 1c) shrinks into a thin layer of ~ 50 μm when dried in an oven at 80 °C (Supplementary Fig. 7). SEM confirms the formation of a dense, tightly packed multilayer film (Figure 2h), which can be explained by the surface tension of water pulling the GO sheets together during evaporation. In contrast, freeze-drying the sample minimizes such effect and helps preserve the porous structure. Interestingly, such phenomena can be utilized as another method to adjust the sample porosity. By first exchanging the solvent within the GO/b-PEI bead to another solvent with lower surface tension, such as

ethanol, hexane, and toluene, and then drying in the oven, we find that it is possible to produce intermediate structures that are lighter than the packed multilayer but still denser than the freeze-dried samples (Figure 2g and i). Although we have discussed only two factors here, namely GO concentration and the drying method, adjusting other parameters such as b-PEI concentration or solvents may also lead to similar behaviors.

One important question regarding the obtained products is how the presence of b-PEI may affect the properties of GO. In particular, as reduced GO (r-GO) is actively pursued for applications such as ultracapacitors, battery electrodes, and sensors, the conductivity and stability of the assembled GO/b-PEI structure after reduction is of strong interest. To address this question, we first examine the content of b-PEI within the product through thermogravimetric analysis (TGA) and X-ray photoelectron spectroscopy (XPS). Samples produced at GO concentration of 8 mg ml^{-1}, identical to those in Figure 1, were used for the analysis. TGA result (Figure 3a) displays two distinct steps, the first corresponding to deoxygenation of GO and the second to decomposition of b-PEI. The deoxygenation of GO starts at a lower temperature compared to pristine GO; this may be possibly due to the interaction of the oxygen-based functional groups of GO with the amine group of b-PEI. From the weight loss, we estimate the amount of b-PEI within the sample to be ~ 35 % in mass. This value was also confirmed by elemental analysis from XPS (Supplementary Fig. 8). A point to note from TGA is that b-PEI almost fully decomposes at temperatures above 400 °C, leaving only a small residue of less than 15 % its original mass. Despite such reactions, the samples are surprisingly stable. For instance, Figure 3b displays a GO/b-PEI bead after thermal treatment at 450 °C under nitrogen atmosphere for 30 minutes. Not much change is

13

noticed to the overall size and shape of the bead and the microscopic porous network is also well preserved. At the same time, the decomposition of b-PEI leads to enhanced conductivity of the reduced GO structure, as shown below.

To examine the influence of b-PEI to conductivity, we reduced the obtained products in four different ways, namely hydroiodic acid (HI) treatment, hydrazine (N_2H_4) treatment, and thermal treatment at 220 °C and 450 °C, and measured their sheet resistances using a four-probe setup (Jandel HM21 model). For this experiment, the GO/b-PEI samples were prepared in film forms rather than beads to avoid the difficulty of measuring round surfaces. Films can be easily produced with small modifications to the experimental setups as will be discussed in the next section. Structure of the samples was well-preserved even after reduction. Furthermore, all samples showed good recovery of conductivity, with the resistances slightly higher but comparable with pure GO films reduced under identical conditions (Figure 3c). In particular, with thermal reduction at 450 °C, the resistance difference between GO/b-PEI and pure GO became quite small, which can be attributed to the decomposition of b-PEI. These results suggest that although the presence of b-PEI may lead to slightly decreased conductivity of the reduced GO, such influence can be minimized by removing the polyelectrolyte through thermal treatments.

Forming GO/b-PEI film on solid/flexible substrates. Up to this point we have mainly examined the dd-LbL assembly using the formation of bead structures by complexation of GO and b-PEI on a liquid droplet surface. However, with simple modifications to the experimental configuration, it is possible to construct a much wider range of 3D architectures.

For example, instead of adding a droplet of b-PEI solution directly into a GO suspension, one can first apply it on a glass substrate as shown in Figure 4a. Note that green dye was added to the solution for easier visualization. When the glass slide is immersed in a GO suspension (8 mg ml^{-1}) for several hours, a thick film forms over the area where the b-PEI droplet was originally applied (Figure 4b). Based on previous discussions, it is reasonable to expect that such film formation is also driven by diffusion of b-PEI from the deposited droplet, or in other words, through dd-LbL assembly. Indeed, the properties and microstructures of such GO/b-PEI films show strong resemblance with those of the beads. When freeze-dried, the overall shape of the film is well-preserved. At the same time, cross-sectional SEM image (Figure 4c) reveals a porous network of GO similar to that observed from the beads (Figure 1). On the other hand, when dried in an oven, the sample shrinks into a tightly packed multilayered film (Figure 4d) due to the surface tension of water pulling the GO sheets together as discussed in Figure 2. In either case, the nanosheets are mostly oriented parallel to the glass slide.

Such preparation of GO/b-PEI film on substrates is quite robust, and we have not yet found much limitation to the type of surface and size of area on which the assembly can be performed. For instance, Figure 4e displays a film formed on filter paper. To get this, b-PEI

solution was first applied to a square area of 8 cm x 10 cm. After immersion in GO suspension, GO/b-PEI film was developed over the same area. The film thickness is fairly uniform throughout the whole sample, as can be noticed from Figure 4f. Other than the dimension of the reaction vessel, we have not found much limitation to the size of film that can be produced. The ability to prepare films in such large areas is potentially useful for practical applications. For example, by cutting the film into smaller pieces (2 cm x 2 cm), we were able to easily obtain sufficient number of samples for testing out various reductions methods as presented in Figure 3c.

It should be noted that formation of the GO/b-PEI film is mostly confined to where the b-PEI has been applied, which is natural since the polyelectrolyte is serving as the main element in driving the assembly and keeping the structure intact. In other words, it becomes possible to create patterned films on a given substrate by applying b-PEI only to pre-determined areas, as shown in Figure 4g. Although this is a simple demonstration, it is not difficult to imagine the preparation of more complex patterns through precise deposition of b-PEI through assistance of conventional techniques such as microfluidics and lithography. Up to now, the patterning of GO on substrates has been mostly limited to single or few layer thin films. The growth of thick multilayered structure, especially with controllable porosity, adds a new dimensionality to the patterning of nanomaterials.

Furthermore, this kind of assembly can also be extended to non-flat surfaces. For example, creating a thick GO/b-PEI layer around a thin thread can be easily achieved by first soaking the tread with b-PEI solution and then immersing it in a GO suspension (Figure 4h). As similar to previous results, drying the sample in an oven leads to formation of a packed

multilayer film as confirmed by SEM (Figure 4i). These results again demonstrate the versatility of the dd-LbL assembly, which can be performed on surfaces with diverse materials, shapes, and sizes, allowing the construction of nanosheets into a wide range of 3D macrostructures.

Tailoring the assembled GO/b-PEI structure using templates. In addition to methods discussed above, the shape of the assembled products can be also controlled by using templates. Figure 5 shows a simple demonstration of such concept. A polydimethylsiloxane (PDMS) slab with a hole in the middle was placed on a glass slide to form a well. A small amount of b-PEI solution was applied to the bottom of the well (Figure 5a), and then the substrate was immersed in a GO suspension for several hours. Complexation of GO and b-PEI occurred within the well driven by diffusion of the polyelectrolyte (Figure 5b). The GO/b-PEI complex could be easily detached from the PDMS slab, and also retained the shape of the template (Figure 5c). Therefore, this provides a simple method to produce free-standing architectures with controllable shapes.

Discussion

In this report, we introduced a strategy for constructing GO sheets into various 3D macrostructures, namely "diffusion driven layer-by-layer (dd-LbL) assembly". This process is based on polyionic complexation of the negatively charged GO and positively charged branched polyethylenimine (b-PEI) at an interface. The key point is that the diffusion of b-PEI across the interface allows the complex layer to continuously grow into macroscopic

structures without additional external stimuli. Interestingly, the GO/b-PEI complex forms a foam-like porous network, which porosity can be tuned from ultra-light (5.6 mg cm^{-3}) to tightly packed (~ 1800 mg cm^{-3}) through simple adjustments in experimental condition. Furthermore, the assembly process can be utilized in various configurations such as to create free-standing architectures with tailored shapes or patterned films on a substrate. The simplicity and versatility of this process should be useful in constructing a wide range of 3D graphene-based architectures. At the same time, we believe that this concept of utilizing the diffusion of polyelectrolyte for the assembly of nanosheets into macrostructures should also be applicable to a much wider range of materials.

Methods

Synthesis of graphene oxide (GO). GO was synthesized using a modified Hummers method reported earlier.[36] In brief, concentrated H_2SO_4 (75 ml) was heated to 80 °C in a 500 ml round bottom flask. $K_2S_2O_8$ (15 g) and P_2O_5 (15 g) were added to the acid and stirred until fully dissolved. Graphite powder (20 g, Bay Carbon Inc. SP-1 grade) was added to the solution and kept at 80 °C for 4.5 h. The mixture was then cooled, diluted with 1.5 L of deionized (DI) water, and filtered using filter papers (Whatman, Grade No.3). The collected product was further rinsed with DI water (6 times, 1 L each), and dried in air. The powder was then transferred into a 2 L Erlenmeyer flask with concentrated H_2SO_4 (750 ml) and cooled down to 5 °C using an ice bath. $KMnO_4$ (100 g) was slowly added to the mixture while stirring. The flask was then transferred to a 35 °C water bath and left for 2 hours, and then transferred back into an ice bath. DI water (1 L) was slowly added to the flask while stirring, taking great

18

caution to keep the temperature below 20 °C. The suspension was left for 2 hours, and diluted with DI water to a total volume of 4 L. 80 ml of a 30 % H_2O_2 solution was slowly added to the flask while stirring, forming orange precipitates. The product was filtered using a PTFE membrane (Millipore, OmniporeTM membrane, 5.0 μm pores), rinsed with 3.4 % HCl solution (1 L at a time, up to a total 6 L), collected and dried in a desiccator with P_2O_5 as drying agent. The solid was redispersed in acetone, filtered using a PTFE membrane (Millipore, FluoroporeTM membrane, 3.0 μm pores), further rinsed with additional acetone (1 L at a time, up to a total 6 L), and dried in ambient conditions. The final product, which is oxidized graphite, was exfoliated into GO by sonicating in water. The exfoliated product was freeze-dried and stored in powder form, which was re-dispersed in DMF/water (9:1) mixture before use.

Formation of GO/b-PEI beads. In general, five to six droplets of b-PEI solution (M_w = 750,000, M_n = 60,000, 25 wt. % in DI, ~ 12 μL) were added to 10 ml of GO suspension (8 mg ml^{-1} in DMF:water = 9:1 mixture) in a 20 ml glass vial using a micropipette. The vial was then left on a shaker for several hours, typically around 24 hours. After that, the samples were rinsed by immersing in DI water for two to three days. The DI water was exchanged three times a day.

Formation of GO/b-PEI films on substrates. Small amount of b-PEI solution (25 wt. % in DI) was applied to the substrate of interest, such as glass slides and filter paper. The substrate was then immersed in a GO suspension (8 mg ml^{-1} in DMF:water = 9:1 mixture) and left on a shaker for several hours, typically around 24 hours. For example, film shown in Figure 4e has

19

been prepared by first applying 1 ml of the b-PEI solution to an 8 cm x 10 cm rectangular area of a filter paper (Whatman, grade 3); the substrate was then immersed in 90 ml of the GO suspension and left on a shaker for 24 hours. A plastic container with dimensions of 15 cm x 10 cm x 5 cm was used as reaction vessel. After the film formation, samples were rinsed by immersing in DI water for two to three days. The DI water was exchanged three times a day. In the case of using a thread as the substrate, the fiber was first immersed in the b-PEI solution for a few seconds and then transferred into a GO suspension. All other procedures are identical.

Drying the assembled GO/b-PEI structures. After rinsing the samples, freeze-drying was used to get porous foam-like structures. Tightly packed films were obtained by drying the samples in an oven at 80 °C for overnight. To prepare structures with intermediate densities, the water in the initial product was exchanged to a solvent with low surface tension such as toluene, hexane, and ethanol. After that, the sample was dried in an oven at 80 °C for overnight.

Sheet resistance measurement of reduced GO/b-PEI films. GO/b-PEI films were prepared on a filter paper (Whatman, grade 3) by the method discussed above. In general, square area of 8 cm x 10 cm was used. The film was dried and then cut into smaller pieces (2 cm x 2 cm), which were reduced in four different ways. 1) Hydroiodic acid (HI) treatment: sample was immersed in a HI solution (55 % in DI) and kept at room temperature for overnight. After that, it was rinsed with ethanol until no more iodine residue (identified by the brown color) was seen coming out. 2) Hydrazine treatment: sample was place in an autoclave with small

amount of hydrazine (2 % in water) and kept at 80 °C for overnight. 3 and 4) Thermal treatment at 220 °C and 450 °C: sample was placed inside a tube furnace under nitrogen atmosphere. Heating rate was 5 °C min^{-1} for both cases. The samples were left at the final temperature for 30 minutes and then taken out. Pure GO films were prepared by placing a PTFE dish containing GO suspension (8 mg ml^{-1}) in an 80 °C oven. The dried GO film was cut into 2 cm x 2 cm pieces and reduced the same way as the GO/b-PEI films.

Sheet resistant of the reduced films was measured by a Jandel HM21 Portable Four Point Probe Test Meter (cylindrical four point probe head, probe spacing 1 mm). Current was set as 10 mA, and sheet resistance was read out from the meter in $\Omega \ \square^{-1}$.

Characterization. Unless mentioned otherwise, data presented in the manuscript has been collected from samples obtained after reaction time of 24 hours. Transmission FT-IR spectra were obtained using a JASCO FT/IR-4200 spectrometer. Measurements were conducted under ambient conditions. Resolution was set to 4 cm^{-1} with scanning range from 400 to 4000 cm^{-1}. Forty-eight scans per samples were recorded, averaged and corrected against the spectrum of pure KBr as background. XRD measurements were performed using a Rigaku RINT2500 with Cu Kα radiation (λ = 0.154 nm). Scanning electron microscope (SEM) images were taken with a JEOL JSM-7001 F4 microscope, using acceleration voltage in the range of 2 to 15.0 kV. Sample was fixed on a silicon wafer or conductive carbon tape. To minimize charging effects, 5 nm layer of osmium was applied to non-conductive samples prior to imaging. Thermogravimetric analyses (TGA) were performed using a Thermo plus EVO II system (Rigaku). In general, samples were freeze-dried before testing. Measurement

21

was done under nitrogen atmosphere (flow rate of 50 ml hour^{-1}) with temperature range of 25 to 500 °C and scan rate of 10 °C min^{-1}. Composition of b-PEI with the assembled structures was determined by comparing the mass loss between 100 and 500 °C.

References

1 Stankovich, S. *et al.* Synthesis of graphene-based nanosheets via chemical reduction of exfoliated graphite oxide. *Carbon* **45**, 1558-1565, (2007).

2 Hernandez, Y. *et al.* High-yield production of graphene by liquid-phase exfoliation of graphite. *Nat. Nanotechnol.* **3**, 563-568, (2008).

3 Ramakrishna Matte, H. S. S. *et al.* MoS_2 and WS_2 analogues of graphene. *Angew. Chem. Int. Ed.* **49**, 4059-4062, (2010).

4 Coleman, J. N. *et al.* Two-dimensional nanosheets produced by liquid exfoliation of layered materials. *Science* **331**, 568-571, (2011).

5 Sasaki, T., Watanabe, M., Hashizume, H., Yamada, H. & Nakazawa, H. Macromolecule-like aspects for a colloidal suspension of an exfoliated titanate. Pairwise association of nanosheets and dynamic reassembling process Initiated from It. *J. Am. Chem. Soc.* **118**, 8329-8335, (1996).

6 Naguib, M. *et al.* Two-dimensional nanocrystals produced by exfoliation of Ti_3AlC_2. *Adv. Mater.* **23**, 4248-4253, (2011).

7 Zhi, C., Bando, Y., Tang, C., Kuwahara, H. & Golberg, D. Large-scale fabrication of boron nitride nanosheets and their utilization in polymeric composites with improved thermal and mechanical properties. *Adv. Mater.* **21**, 2889-2893, (2009).

8 Stoller, M. D., Park, S., Zhu, Y., An, J. & Ruoff, R. S. Graphene-based ultracapacitors. *Nano Lett.* **8**, 3498-3502, (2008).

9 Yoo, J. J. *et al.* Ultrathin planar graphene supercapacitors. *Nano Lett.* **11**, 1423-1427, (2011).

10 Sugimoto, W., Iwata, H., Yasunaga, Y., Murakami, Y. & Takasu, Y. Preparation of ruthenic acid nanosheets and utilization of its interlayer surface for electrochemical energy storage. *Angew. Chem. Int. Ed.* **42**, 4092-4096, (2003).

11 Yoo, E. *et al.* Large reversible Li storage of graphene nanosheet families for use in rechargeable lithium ion batteries. *Nano Lett.* **8**, 2277-2282, (2008).

12 Kulkarni, D. D., Choi, I., Singamaneni, S. S. & Tsukruk, V. V. Graphene oxide−polyelectrolyte nanomembranes. *ACS Nano* **4**, 4667-4676, (2010).

13 Lee, K., Gatensby, R., McEvoy, N., Hallam, T. & Duesberg, G. S. High-performance sensors based on molybdenum disulfide thin films. *Adv. Mater.* **25**, 6699-6702, (2013).

14 Late, D. J. *et al.* Sensing behavior of atomically thin-layered MoS_2 transistors. *ACS Nano* **7**, 4879-4891, (2013).

15 Liu, S. *et al.* Antibacterial activity of graphite, graphite oxide, graphene oxide, and reduced graphene oxide: membrane and oxidative stress. *ACS Nano* **5**, 6971-6980, (2011).

16 Tung, V. C. *et al.* Low-temperature solution processing of graphene−carbon nanotube

hybrid materials for high-performance transparent conductors. *Nano Lett.* **9**, 1949-1955, (2009).

17   Eda, G., Fanchini, G. & Chhowalla, M. Large-area ultrathin films of reduced graphene oxide as a transparent and flexible electronic material. *Nat. Nanotechnol.* **3**, 270-274, (2008).

18   Yang, X. *et al.* Ordered gelation of chemically converted graphene for next-generation electroconductive hydrogel films. *Angew. Chem. Int. Ed.* **50**, 7325-7328, (2011).

19   Sasaki, T., Ebina, Y., Watanabe, M. & Decher, G. Multilayer ultrathin films of molecular titania nanosheets showing highly efficient UV-light absorption. *Chem. Comm.*, 2163-2164, (2000).

20   Podsiadlo, P. *et al.* Exponential growth of LBL films with incorporated inorganic sheets. *Nano Lett.* **8**, 1762-1770, (2008).

21   Cote, L. J., Kim, F. & Huang, J. Langmuir−Blodgett assembly of graphite oxide single layers. *J. Am. Chem. Soc.* **131**, 1043-1049, (2008).

22   Li, X. *et al.* Highly conducting graphene sheets and Langmuir-Blodgett films. *Nat. Nanotechnol.* **3**, 538-542, (2008).

23   Xu, Y., Sheng, K., Li, C. & Shi, G. Self-assembled graphene hydrogel via a one-step hydrothermal process. *ACS Nano* **4**, 4324-4330, (2010).

24   Wu, Z.-S. *et al.* Three-dimensional nitrogen and boron co-doped graphene for high-performance all-solid-state supercapacitors. *Adv. Mater.* **24**, 5130-5135, (2012).

25   Zhao, Y. *et al.* A Versatile, Ultralight, Nitrogen-Doped Graphene Framework. *Angew. Chem. Int. Ed.* **51**, 11371-11375, (2012).

26   Liu, L. *et al.* Nanostructured Graphene Composite Papers for Highly Flexible and Foldable Supercapacitors. *Adv. Mater.* **26**, 4855-4862, (2014).

27   Imperiali, L., Clasen, C., Fransaer, J., Macosko, C. W. & Vermant, J. A simple route towards graphene oxide frameworks. *Mater. Horiz.* **1**, 139-145, (2014).

28   Niu, Z., Chen, J., Hng, H. H., Ma, J. & Chen, X. A leavening strategy to prepare reduced graphene oxide foams. *Adv. Mater.* **24**, 4144-4150, (2012).

29   Si, Y. & Samulski, E. T. Exfoliated graphene separated by platinum nanoparticles. *Chem. Mater.* **20**, 6792-6797, (2008).

30   Kim, H., Miura, Y. & Macosko, C. W. Graphene/polyurethane nanocomposites for improved gas barrier and electrical conductivity. *Chem. Mater.* **22**, 3441-3450, (2010).

31   Zou, J. & Kim, F. Self-assembly of two-dimensional nanosheets induced by interfacial polyionic complexation. *ACS Nano* **6**, 10606-10613, (2012).

32   G. Babak, V., A. Merkovich, E., S. Galbraikh, L., V. Shtykova, E. & Rinaudo, M. Kinetics of diffusionally induced gelation and ordered nanostructure formation in surfactant-polyelectrolyte complexes formed at water/water emulsion type interfaces. *Mendeleev Commun.* **10**, 94-95, (2000).

33   Capito, R. M., Azevedo, H. S., Velichko, Y. S., Mata, A. & Stupp, S. I. Self-assembly of large and small molecules into hierarchically ordered sacs and membranes. *Science* **319**, 1812-1816, (2008).

34   Gunes, D. Z., Pouzot, M., Rouvet, M., Ulrich, S. & Mezzenga, R. Tuneable thickness barriers for composite o/w and w/o capsules, films, and their decoration with particles. *Soft Matter* **7**, 9206-9215, (2011).

35   Chen, Z. *et al.* Three-dimensional flexible and conductive interconnected graphene networks grown by chemical vapour deposition. *Nat. Mater.* **10**, 424-428, (2011).

36   Kim, F. *et al.* Self-propagating domino-like reactions in oxidized graphite. *Adv. Funct. Mater.* **20**, 2867-2873, (2010).

Author contributions

J. Z. performed the experiments, interpreted the data and wrote the manuscript. F. K. conceived the study and wrote the manuscript.

Competing financial interests. The authors declare no competing financial interests.

Additional information. Supporting Information accompanies this paper at http://www.nature.com/naturecommunications.
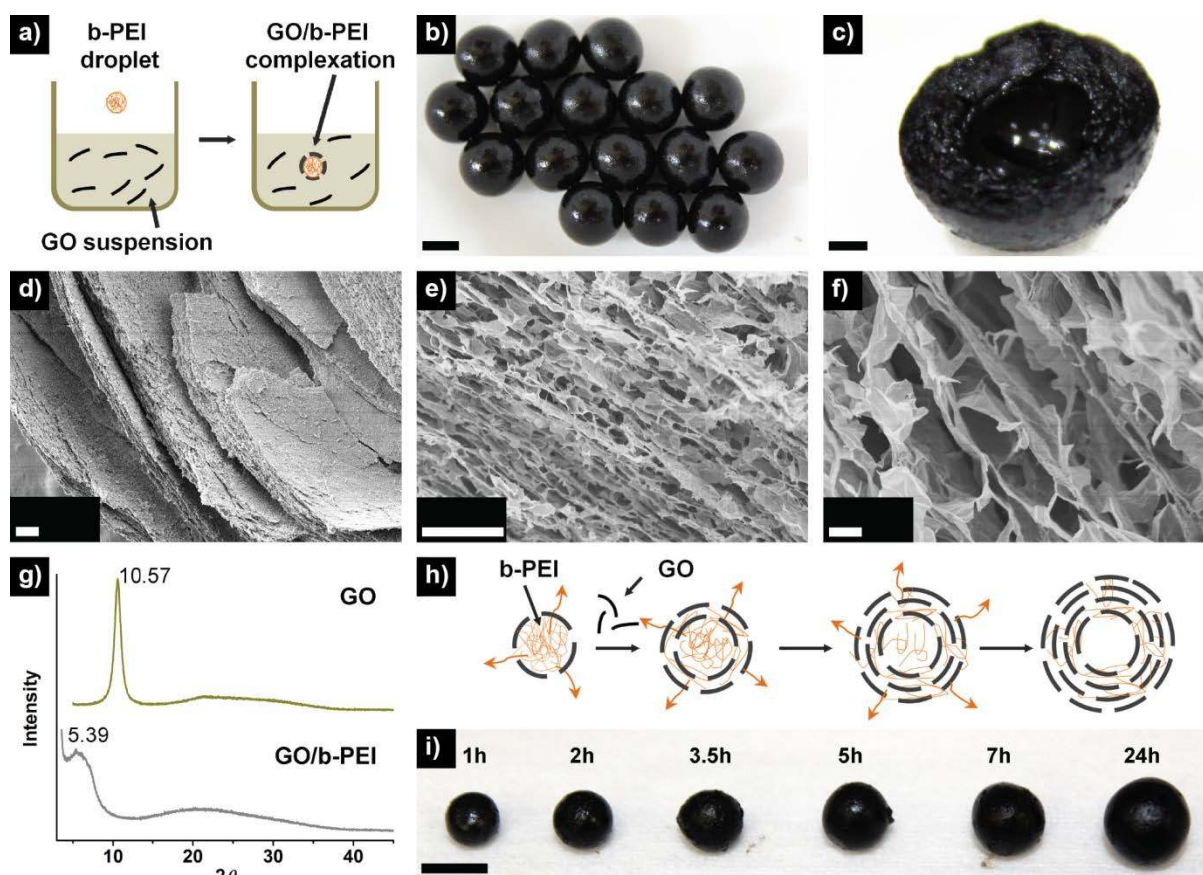
Figure 1. Diffusion driven layer-by-layer assembly of graphene oxide. a) Schematic representation of an experimental setup. When droplets of branched polyethylenimine (b-PEI) solution are added to a graphene oxide (GO) suspension, complexation between b-PEI and GO occurs at the droplet surface. This results in the formation of stable bead-like structures (**b**). **c**) Cross-section of a bead shows that the layer of GO/b-PEI complex is a few millimeters thick. Furthermore, from SEM images (**d-f**) we find the nanosheets form a layered and porous network. **g**) XRD analysis reveals an increase of interlayer distance in GO, suggesting that b-PEI is serving as a binder between the nanosheets. **h**) Proposed assembly mechanism. Key point is the ability of b-PEI to diffuse through the GO/b-PEI complex, which allows continuous growth of the layer into thick macrostructures without any additional treatments. **i**) Longer reaction time produces larger beads, supporting the hypothesis that the assembly is driven by the diffusion of b-PEI. Scale bar, (**b**) 5 mm, (**c**) 1 mm, (**d**) 100 μm, (**e**) 10 μm, (**f**) 1 μm, and (**i**) 5 mm.

27
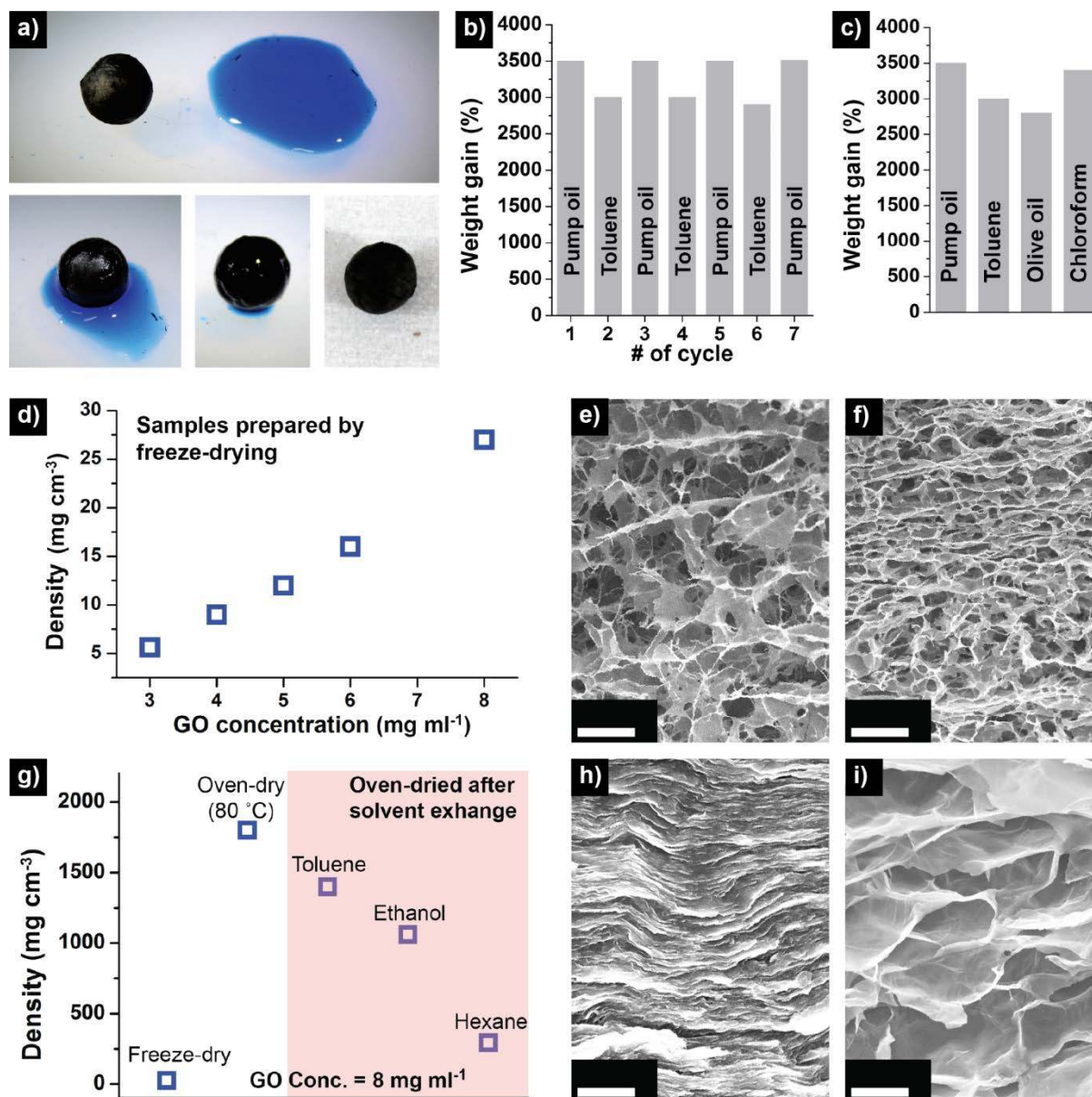
Figure 2. Porosity of the GO/b-PEI beads produced by dd-LbL assembly. a) When placed on top of a pool of pump oil, the GO/b-PEI bead rapidly absorbs the oil due to its porous nature. The bead can be recycled by immersing it in hexane to drain the absorbed oil and then drying it under ambient conditions (bottom right). **b**) Oil absorption experiment alternating between pump oil and toluene. Even after several cycles there is no noticeable change in the absorption efficiency, demonstrating its structural stability. **c**) Similar absorption efficiency is observed for other non-polar solvents. **d**) Density of the beads

28

prepared from GO suspensions of varying concentrations. Lower GO concentrations result in beads with lower densities, or in other words, higher porosity. This is confirmed by SEM, with (**e**) and (**f**) displaying samples prepared with concentrations of 3 mg ml^{-1} and 5 mg ml^{-1}, respectively. These samples were dried by freeze-drying. (**g**) However, using different drying method can also influence the porosity. For example, when dried in an 80 °C oven, the surface tension of water pulls the GO sheets together into a densely packed multilayered film (**h**). Intermediate densities can also be achieved by exchanging the water to solvents with lower surface tension, such as hexane, before drying (**i**). Scale bar, (**e**, **f**) 10 μm and (**h**, **i**) 1 μm.
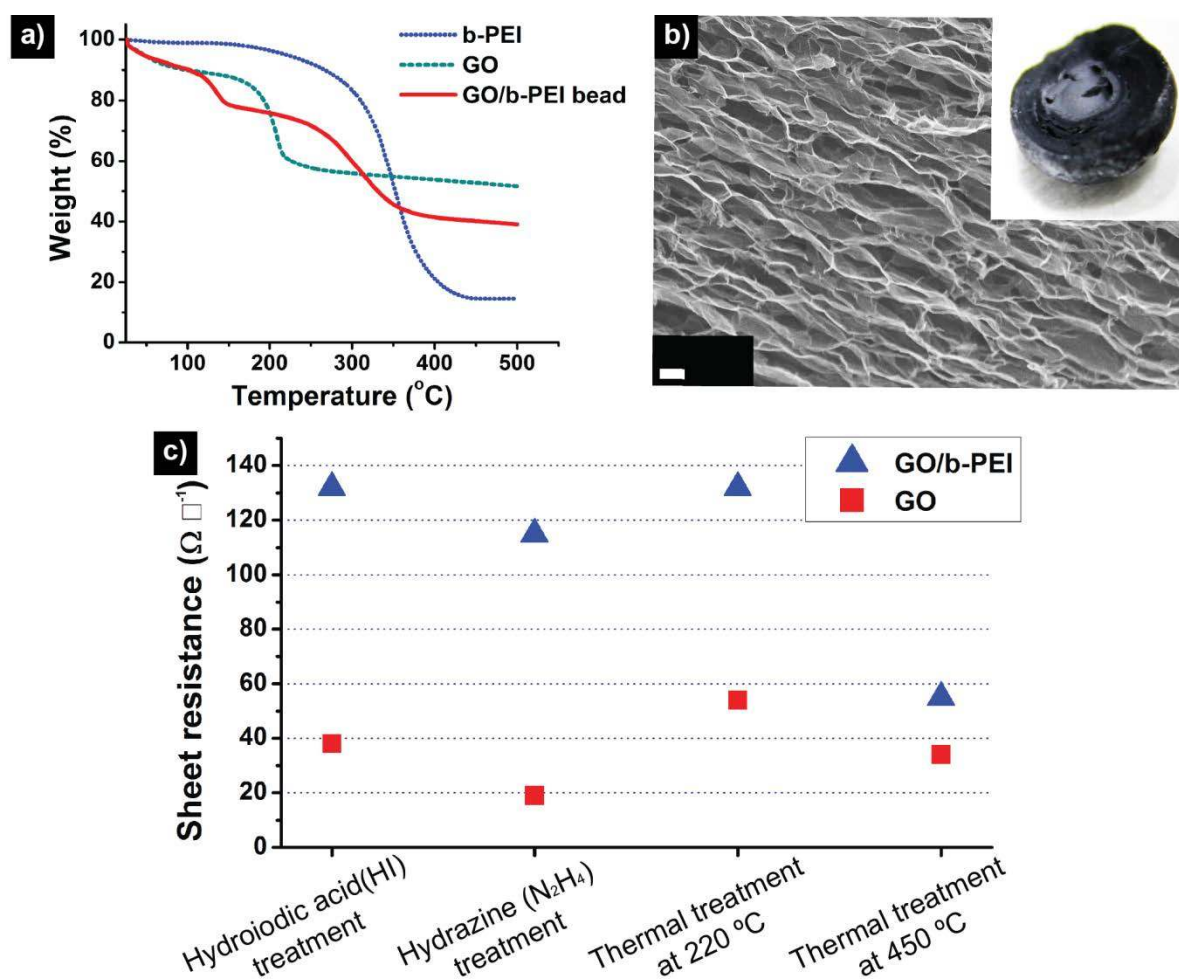
Figure 3. Properties of the assembled GO/b-PEI structures. a) From thermogravimetric analysis (TGA), the composition of b-PEI within a GO bead can be estimated to be ~ 35 % in mass. At the same time, the result implies that significant portion of b-PEI becomes decomposed at temperatures above 400 °C. **b**) Despite such reactions, the samples show good thermal stability. Image shows a GO/b-PEI bead after thermal treatment at 450 °C. Not much change is noticed in both the porous framework and overall structure (inset). **c**) The assembled GO/b-PEI structures can be reduced using various methods, after which the sheet resistances become slightly higher but comparable to pure GO samples reduced under identical conditions. In particular, the samples which were thermally treated at 450 °C show improved conductivity, which is likely due to decomposition of b-PEI. Scale bar, (**b**) 1μm.
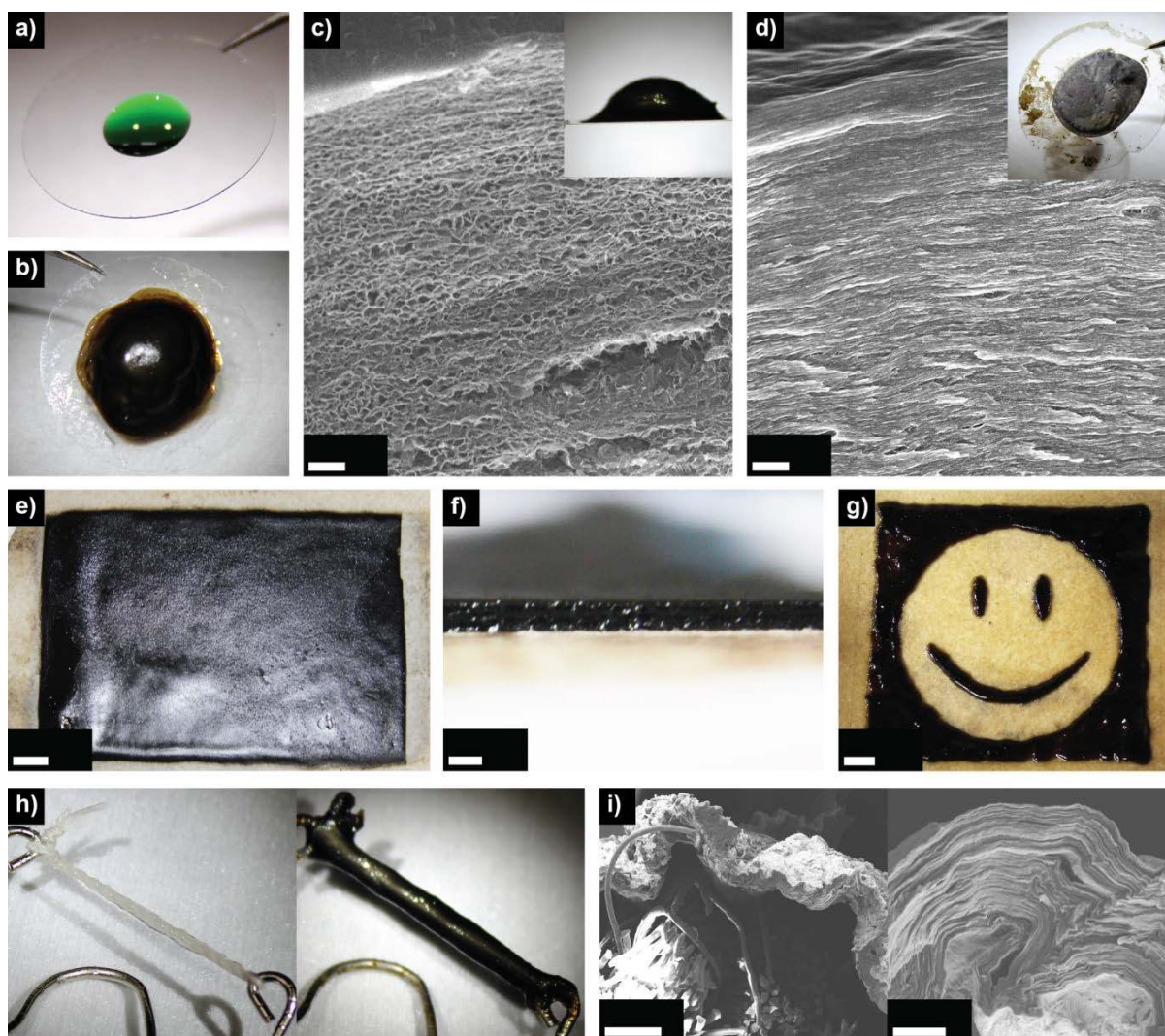
Figure 4. Forming GO/b-PEI films on solid and flexible substrates. a-d) Demonstration on a glass slide. **a**) A drop of b-PEI solution is first deposited onto the substrate. **b**) When the glass slide is immersed in a GO suspension, a thick film develops over that area. As in the case of beads (Figure 2), freeze-drying the sample provides a porous foam-like structure (**c**), whereas oven drying gives a packed multilayered film (**d**). **e**) Large area (8 cm x 10 cm) film prepared on a filter paper using a similar procedure. Film thickness is fairly uniform throughout the sample (**f**). The GO/b-PEI film forms only on the area to where b-PEI was applied, which allows patterning of the film into pre-determined shapes (**g**). **h-i**) This assembly can also be performed on non-flat surfaces, such as a thin thread. **i**) Cross-sectional SEM confirms the formation of a multilayer coating around the thread. Scale bar, (**c**) 5 μm, (**d**) 1 μm, (**e**) 1 cm, (**f**) 1 mm, (**g**) 1 cm, (**i**, left) 100 μm, and (**i**, right) 10 μm.
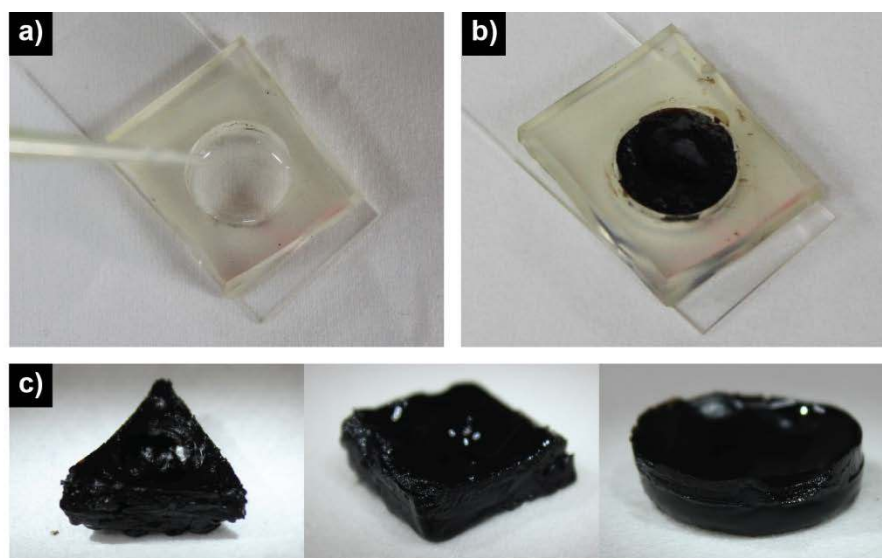
31

222

Figure 5. Tailoring the assembled GO/b-PEI structure using templates. a) A PDMS slab with a hole is placed on a glass slide to form a well, to which a small amount of b-PEI solution is applied. **b**) When the slide is immersed in a GO suspension, complexation between GO and b-PEI occurs within the confined space and forms a stable macrostructure. **c**) The resulting products can be easily released from the template as free-standing pieces. Furthermore, shape of the GO/b-PEI structures closely follows that of the template, allowing the production of diverse forms.
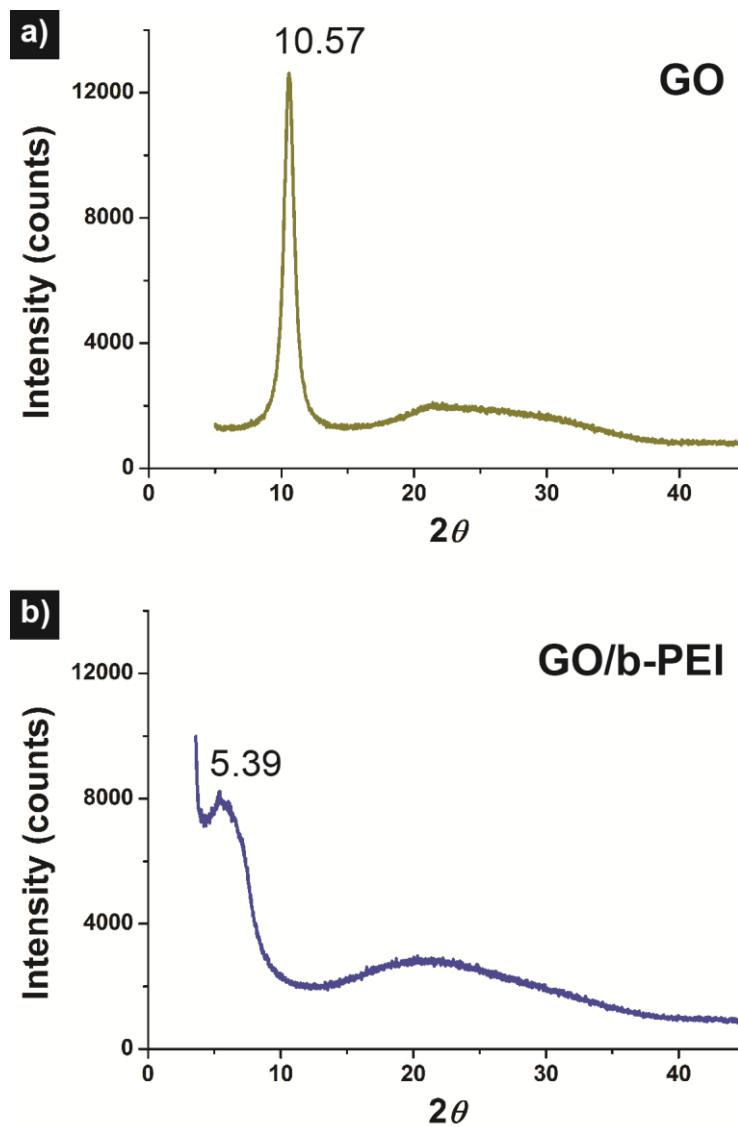
Supplementary Figure 1. X-ray diffraction spectra of pristine GO and GO/b-PEI complex (enlargement of Figure 1g). The interlayer spacing between GO sheets (top, $2\theta = 10.57°$, $d = 0.84$ nm) significantly increases after complexation with b-PEI (bottom, $2\theta = 5.39°$, $d = 1.64$ nm), suggesting that the b-PEI becomes incorporated between GO layers during the assembly process.
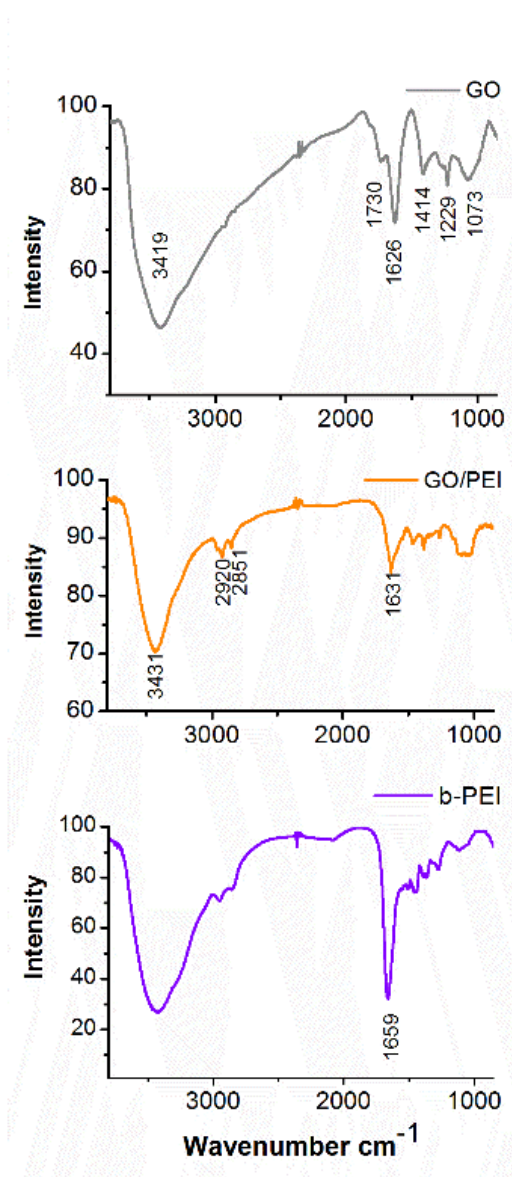
Supplementary Figure 2. FT-IR spectra of pristine GO (top), GO/b-PEI complex (middle) and b-PEI (bottom). Pristine GO shows a peak at 1730 cm^{-1} and 1626 cm^{-1} from C=O (carbonyl) stretching and C=C (aromatic) stretching, respectively. However, the carbonyl peak becomes no longer noticeable after complexation with b-PEI. In addition, characteristic peak from the amine group of b-PEI (1659 cm^{-1}) is also not observed from the complex.

a)

Reaction time (hours)	2	4	6	8	10	12	14	16	18	20	22	24
Bead diameter (mm)	5.12	5.61	5.69	6.22	6.34	6.6	6.7	6.73	6.81	6.88	7.02	7
GO/b-PEI layer thickness (mm)	1.19	1.61	1.67	1.8	1.85	1.95	2.1	2.07	2.08	2.17	2.26	2.29
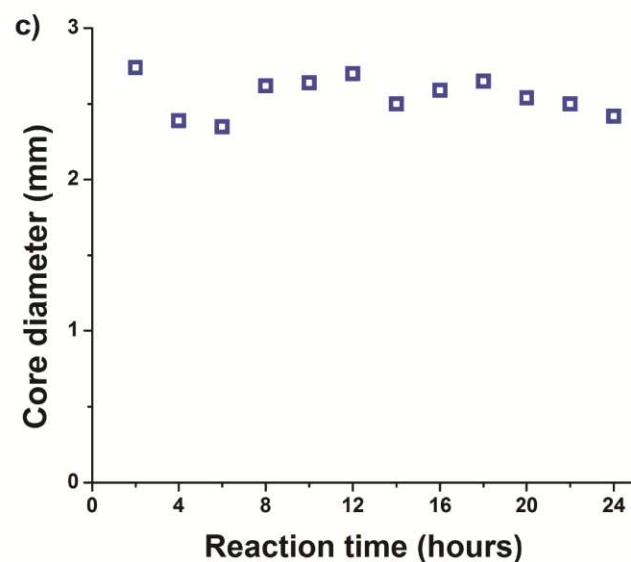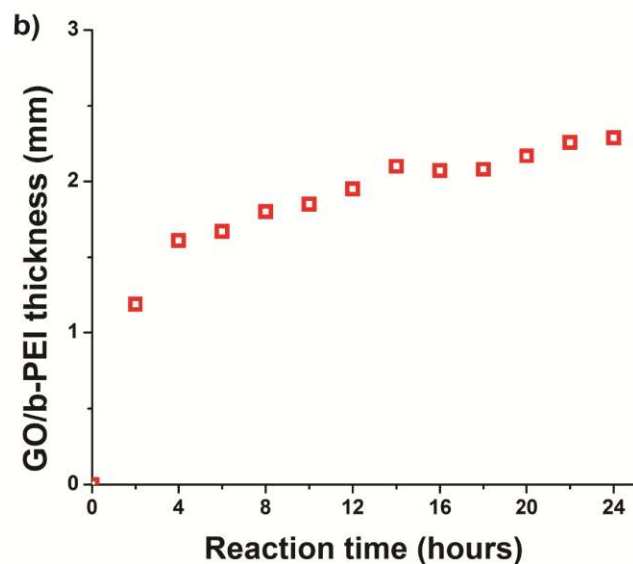
**Supplementary Figure 3. Growth rate of the GO/b-PEI complex layer during bead formation.** a) Bead size and the GO/b-PEI complex layer thickness with varying reaction times. Samples were freeze-dried prior to measurement. b) Most of the GO/b-PEI growth occurs within the first 10 hours (~ 85%) and then eventually slows down with time, with no noticeable changes after 24 hours. Such decline in growth is expected due to depletion of b-PEI and increased distance of diffusion. c) In contrast, the size of the hollow core stays more or less constant during the assembly (2.55 mm ± 0.12 mm), suggesting that the GO/b-PEI complexation first occurs at the surface of b-PEI solution droplet and then grows outwards due to diffusion of the polyelectrolyte.

3
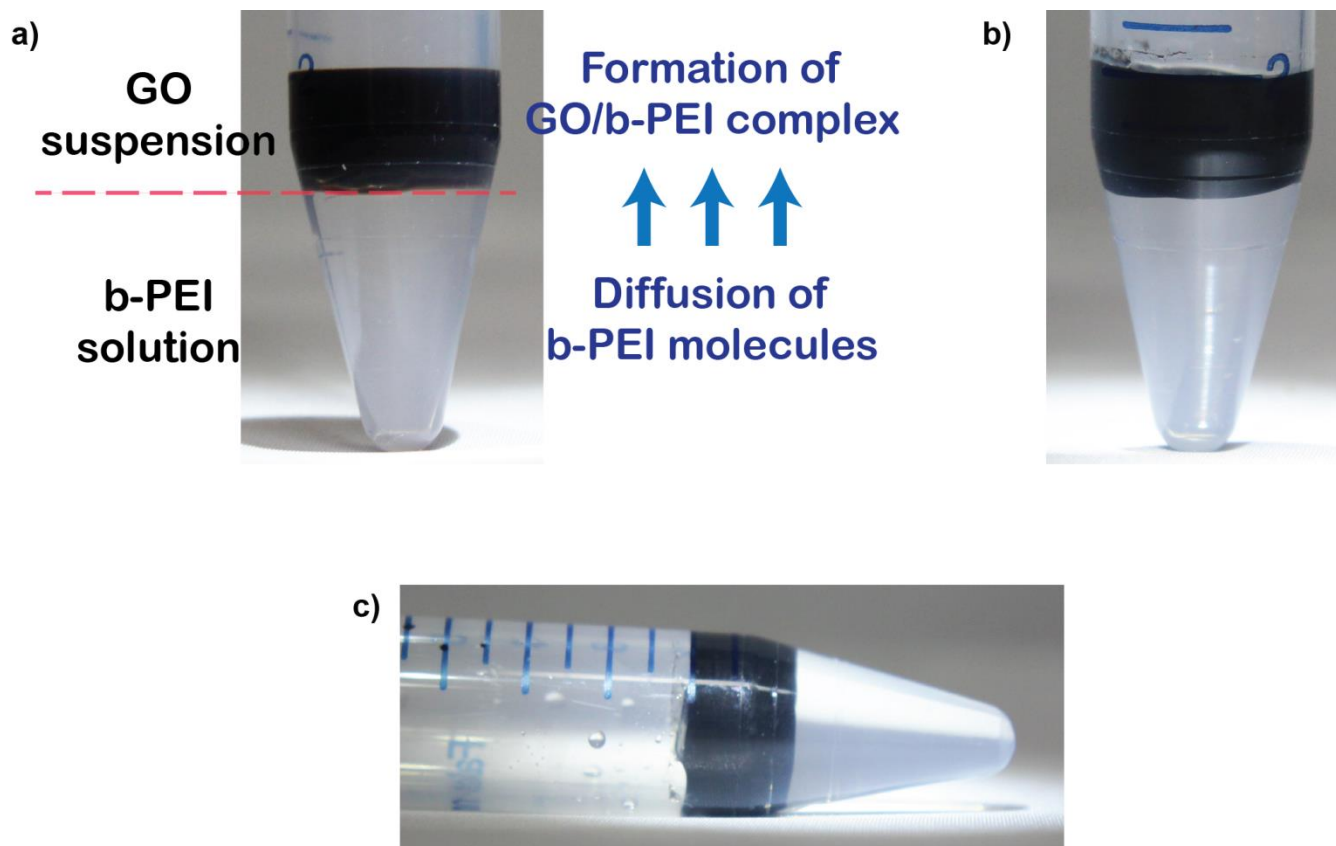
Supplementary Figure 4. Interfacial complexation between GO and b-PEI within a transparent tube. a) Experimental setup. First, 1 ml of b-PEI solution (25 wt. % in DI) was added to a 15 ml centrifuge tube. Then, 1 ml of GO suspension (8 mg ml^{-1} in DMF:water = 9:1 mixture) was gently added to the same tube such that a stable liquid-liquid interface was formed. After two days, the GO suspension turned into a stable layer which could maintain its shape even when tilted (b and c). This suggests that b-PEI molecules diffused into the GO suspension to form a GO/b-PEI complex. At the same time, no complexation is observed on the b-PEI side, implying that GO sheets are not able to diffuse into the b-PEI solution, which is expected due to the large size of the sheets.

Supplementary Figure 5. Effect of b-PEI concentration on GO/b-PEI bead formation. Image shows the beads produced when a 10 wt. % b-PEI solution was applied to a GO suspension, rather than the 25 wt. % solution used for preparing samples shown in Figure 1. The resulting beads are not only smaller in size but also irregular in shape. When b-PEI solutions with even lower concentrations were used, no stable structure was formed. Scale bar, 5mm.
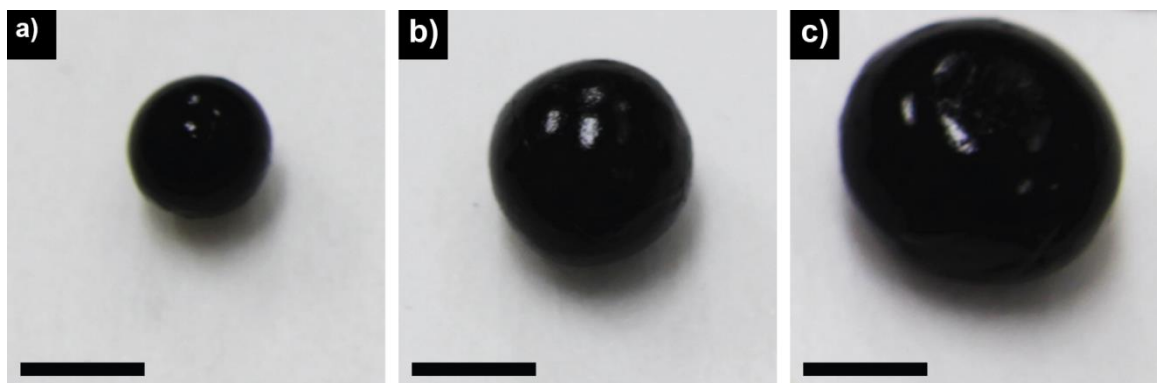
Supplementary Figure 6. Effect of GO concentration on GO/b-PEI bead formation. GO/b-PEI beads produced by GO suspensions with varying concentrations of a) 8 mg ml^{-1}, b) 5 mg ml^{-1}, and c) 3 mg ml^{-1}. Other experimental conditions are identical to those used for preparing samples shown in Figure 1. At lower GO concentrations, b-PEI molecules are able to diffuse longer distances before getting into contact with GO sheets and form a stable complex. Therefore the final assembled structures are larger, as can be easily noticed from the images. It should be noted that while the GO/b-PEI complex layer grows faster at lower GO concentration, it also becomes more loosely packed (i.e., more porous) as shown in Figure 2d-f. Scale bar, (a-c) 5 mm.
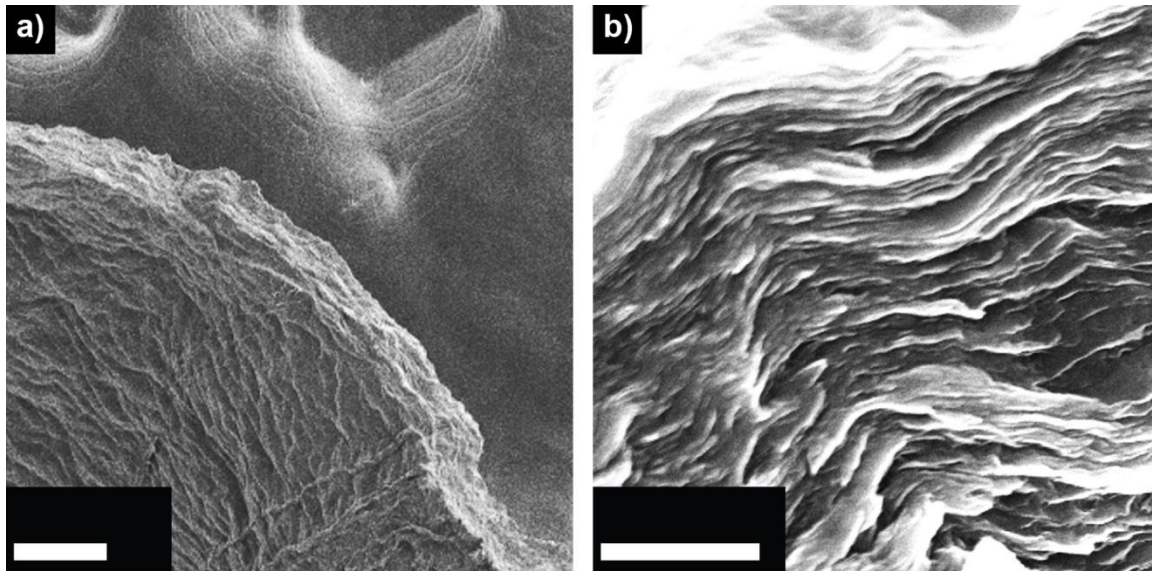
Supplementary Figure 7. GO/b-PEI layer after oven-drying. a) After a bead shown in Figure 1 was dried in an 80 °C oven, the GO/b-PEI layer which thickness was ~ 2 mm in its initial wet state (Figure 1c) shrinks into a thin layer of ~ 50 μm. b) Higher magnification image shows that the GO sheets are pulled together into a packed multilayer film. Scale bar, a) 100 μm, and b) 1 μm.
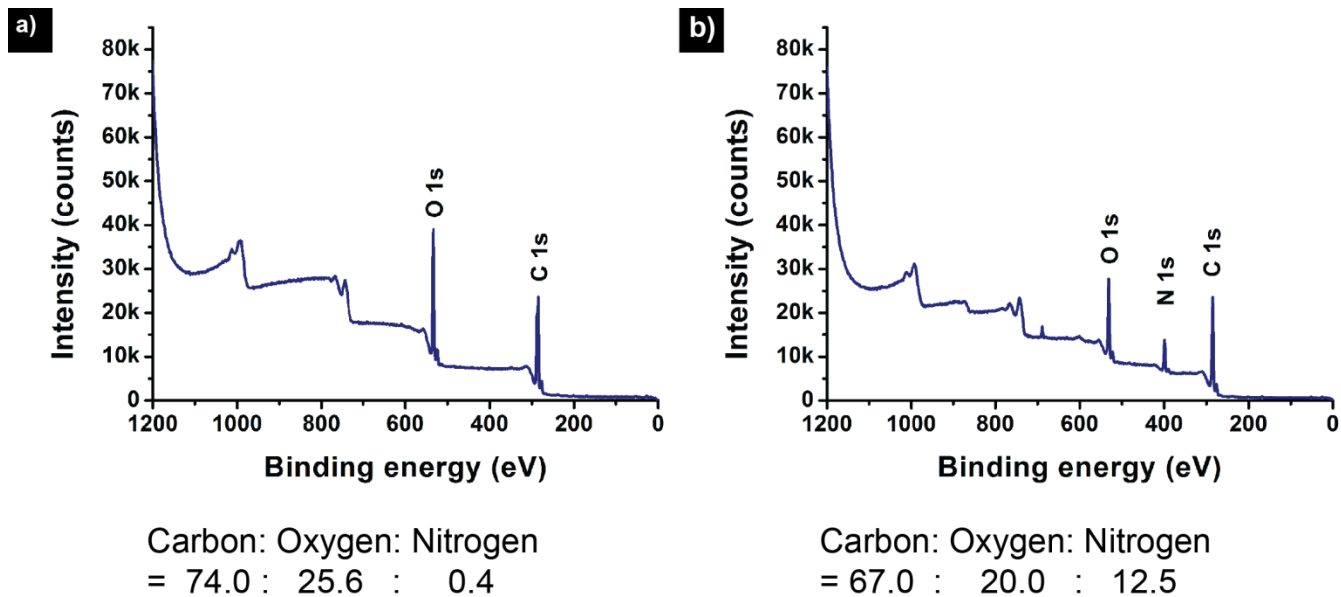
Supplementary Figure 8. Elemental analysis of GO/b-PEI complex by X-ray photoelectron spectroscopy (XPS). XPS from a) pure GO and b) GO/b-PEI complex. From this we can estimate the composition of b-PEI in the assembled structure to be ~ 35 % in mass, which matches with the results from thermogravimetric analysis (TGA, Figure 3a).